Article type: Full Paper

Fabrication and characterization of epitaxial Gd-doped SBN thin films

*Ka Kin Lam, Ka Ho Chan, Sheung Mei Ng, Hon Fai Wong, Yu Kuai Liu, Chi Wah Leung, Chee Leung Mak**

Department of Applied Physics, The Hong Kong Polytechnic University, Hung Hom, Kowloon, Hong Kong, People's Republic of China
E-mail: apaclmak@polyu.edu.hk

Gd-doped $Sr_{0.5}Ba_{0.5}Nb_2O_6$ (SBN50) thin films with Gd-doping concentration ranging from 1 % to 4 % were grown on Pt-coated MgO (100) substrates using pulsed laser deposition technique. X-ray diffraction studies showed that the films were highly (001)-oriented and epitaxially grown on the substrates. Electrical measurements showed that the Gd-SBN films possessed good ferroelectric properties. Ramanent polarization of $+Pr$ = 1.36 μCcm^{-2} and $-Pr$ = -5.73 μCcm^{-2} and coercive field of $+Ec$ = 158.0 kV and $-Ec$ = -30.8 kV were obtained.

1. Introduction

Strontium Barium niobite $Sr_xBa_{1-x}Nb_2O_6$ is a relaxor ferroelectric material with tetragonal tungsten bronze (TTB) structure possessing large linear electro-optic [1] and pyroelectric [2-3] coefficients. It is a solid solution of $SrNb_2O_6$ (SNO) and $BaNb_2O_6$ (BNO) in the range from x = 0.25 to 0.75 compositions. The general chemical formula of TTB structure is ($A1_x$, $A2_{1-x}$, C) M_2O_6 [4]. The Sr cations and Ba cations occupy the A1 and A2 sites respectively, and the C-sites remain vacant. The TTB structure of SBN provides a great variability for structural modification. For example by doping rare-earth elements to replace the A1 and A2 site cations [5] or adding small size cations such as sodium and potassium into the interstitial C-site [6].

Previous studies reported the enhanced ferroelectric and pyroelectric properties of SBN ceramics due to doping with rare-earth elements[7]. For example, Gd-doped SBN ceramics showed a large enhancement (>3 times) in pyroelectric coefficients and relatively low dielectric loss, resulting a large figure of merit (FOM) of detectivity. However, bulk ceramics have limited applications due to their size cannot be reduced into microstructural dimension. On the other hand, solid-state thin film devices have been shown to be applied in larger electrical field and faster heating oscillation applications compared with bulk ceramics. The size of thin film devices can be shrunk into micron-size and integrated on different conventional substrates like silicon or strontium titanate. This paper reports the fabrication and characterization on ferroelectric and dielectric properties of epitaxial Gd-doped SBN50 thin films grown by pulsed laser deposition (PLD) method.

2. Experimental section

Gd-doped SBN50 ($(Sr_{x-3y/2}, Gd_y) Ba_{1-x} Nb_2O_6$, x=0.5 and y= 0.01, 0.02 and 0.04 ceramic target was fabricated by conventional solid-state reaction through mixing strontium carbonate ($SrCO_3$), barium carbonate ($BaCO_3$), niobium pentoxide (Nb_2O_5) and gadolinium (III) oxide (Gd_2O_3) with designated compositions. The mixed powders were ball-milled in ethanol for 8 hours. The collected powders were pressed into a pellet which was calcinated at 1150 ^oC for 10 hours and then sintered at 1300 ^oC for another 10 hours with a ramping rate of 5 ^oC/min. The sintered SBN50 targets with different Gd doping concentrations were then employed for thin film deposition.

Gd-doped SBN50 thin films were grown on Pt-coated (100) MgO substrates by pulsed laser deposition (PLD). The chamber was first evacuated to high vacuum of 10^{-6} mtorr. A 50 nm Pt thin film was first deposited at 700 ^oC with 10 Hz laser pulse repetition rate and 300 mJ laser energy at high vacuum. The targets were ablated by a Lambda Physik KrF Excimer laser operated at 248 nm wavelength. The substrate to target distance was kept at 5 cm. The 500 nm SBN film was then grown in-situ on top of the Pt film with 650 ^oC substrate temperature and 26 Pa oxygen pressure. Substrate to SBN target distance was kept at 4.5 cm. Laser energy was kept at 220 mJ. The deposition of the SBN films was divided into three stages: the first stage employed 2 Hz laser repetition rate for 1800 pulses to slowly grow a 50 nm template layer of SBN. In the second stage the laser repetition rate was changed to 5 Hz to rapidly grow the SBN film. In the final stage, the repetition rate was changed back to 2 Hz to improve the surface roughness of the SBN film. The SBN thin film together with the Pt electrode was then annealed *in-situ* at the same growth temperature for 10 min to improve the crystalline structure. Finally, an Au (50 nm)/Ti (5 nm) thin film was deposited on SBN thin film using E-beam evaporation as top electrodes. The 5 nm titanium served as an adhesion layer to improve the adhesion of the gold film.

To investigate the crystallinity and epitaxy relationship of Gd-SBN50 thin films, X-ray diffraction (XRD) spectroscopy (Rigaku smartlab x-ray diffractometer with a CuKa radiation source with wavelength of 0.1542 nm) was employed. The thin film cross-sections were observed by scanning electron microscope (TESCAN VEGA 3). The ferroelectric hysteresis loop (P-E loop) was measured by a ferroelectric tester (RT66 Radiant Technology)

3. Result and discussion

3.1. GSBN ceramic target characterization

The θ-2θ patterns of the SBN targets with polycrystalline microstructure were shown in **Figure 1.** All the diffraction peaks (black lines) were matched with the SBN50 powder diffraction data. The SBN was crystallized in the tetragonal structure with space group P4bm. The lattice parameters of the SBN ceramics were estimated using the SBN (311) peak (2θ =32.10^o) and (002) peak (2θ =45.85^o). The lattice parameters of a-axis and c-axis were calculated by Bragg's diffraction equation:

$$2d_{hkl} \sin\theta = n\lambda \quad (1)$$

And the interplanar spacing for tetragonal lattice was given by:

$$\frac{1}{d_{hkl}^2} = \frac{h^2 + k^2}{a^2} + \frac{l^2}{c^2} \quad (2)$$

On the basis of our XRD data, the estimated lattice constants a≈b≈1.25 nm and c≈0.39 nm.

Figure 2 shows the θ-2θ scans of SBN thin films deposited on MgO (100) substrates with different Gd-doping concentrations. SBN (001) and (002) peaks are identified with no trace of other reflections, indicating that the SBN films are of single phase. The peak positions of SBN (002) peak of undoped, 1 %, 2 % and 4 % Gd doping are 45.86^o, 45.89^o 45.90^o and 45.97^o respectively. **Table 1** shows the calculated c-lattice constant against the doping concentration. This XRD result shows that when the Gd-doping concentration increased, the SBN (002) peak shifted to a larger angle direction. Since the ionic radius of Gd^{3+} ion is 111 pm which is similar to the Sr^{2+} ion 127 pm, the Gd_2O_3 dopant is likely to replace the Sr^{2+} ion in the doping.[2] When doping concentration increases, the replacement of smaller ionic radius Gd^{3+} will cause the c-lattice constant contract. Similar shifting in diffraction peaks properties had also been reported in cerium-doped SBN ceramics.[5]

3.2. GSBN ferroelectric device fabrication

To study the ferroelectric properties of SBN thin film, a top electrode is needed. **Figure 4** is the schematic diagram of SBN ferroelectric device structure. The bottom and top electrodes were perpendicularly crossed to avoid the direct contact of top and bottom electrode in the wire bond

process. Platinum was used as the bottom electrode because Pt had been demonstrated that it can be grown epitaxially on MgO (001) substrates.[8-9] This Pt thin film does not only act as the bottom electrode, but also helps TTB structured SBN grow epitaxially on the Pt-coated MgO substrate. Because the deposition of SBN thin film needs an oxygen rich atmosphere and high temperature, its high resistance against oxidation also allows the Pt layer maintain good conductivity after the deposition of SBN film.[10]

A scanning electron microscope (SEM) was employed to characterize the cross-section morphologies of the heterostructures. From the cross-section SEM micrograph shown in **Figure 5,** two discernable layers are observed, and the interface between the GSBN thin film and the Pt layer is smooth and sharp. From Figure 5, the thickness of the GSBN and Pt layers are estimated to be 500 nm and 50 nm, respectively.

Figure 6 shows the XRD θ-2θ scan profile of the GSBN/Pt/MgO heterostructure. The Pt thin film is orientated in (002) lattice plane (2θ = 46.12^o) instead of (111) lattice plane (2θ = 39.68^o). The (111) phase of Pt is barely observed because the Pt film was deposited at 700 ^{o}C, and this temperature favors the (001)-orientation instead of (111)-orientation growth due to relatively lower interfacial energy as reported by McIntyre et al.[11], thus the observed Pt film shows the dominated (002) phase in our deposition process. Furthermore, the lattice constants of Pt (a_{Pt} = 0.392 nm) and SBN ($c_{SBN} \approx$ 0.39 nm) are very close, their (002) peaks overlap with each other as observed in Figure 6. Besides the Pt and MgO peaks, SBN (001) and (002) peaks are identified with no trace of other reflections indicating that the SBN film is single phase. The ω-scan rocking curves, shown in the inset of Figure 6 are used to gauge the orientation quality of the films. The full-width half-maximum (FWHM) of Pt (002) and SBN (001) are 0.43^o and 1.64^o, respectively.

X-ray 360^o ϕ-scans of MgO (111), Pt (111) and SBN (221) are plotted in **Figure 7a.** Coincident of the maxima of Φ-scans between Pt (111) and MgO (111) indicates the sequential cube-on-cube growth of Pt-on-MgO. Two sets of in-plane orientation rotation of ± 45^o and ± 56^o from the substrate are observed. It is believed that SBN thin film with (221) lattice was epitaxial grown on Pt (111) thin film, showing a similar behavior as observed in SBN films grown on LSCO (111) thin film with two sets of in-plane orientations [12] due to the similarity in lattice constants between Pt and LSCO. However, the observed values are different from that observed in the epitaxial relationship between MgO (001) substrate and SBN thin film with the in-plane rotations of 18^o and 31^o.[8, 13] The difference in the alignment angle may be caused by the lattice misorientation of the lattice (a_{MgO} = 0.421 nm) or the lattice distortion due to elastic strain on the films.[14] Indeed, the in-plane orientation

rotation of SBN had been reported with different values, [15-18] and it is believed that the orientations are strongly dependent on the processing conditions of the PLD process.

Schematic diagram in **Figure 7b** illustrates the epitaxial relationship and the in-plane orientation of MgO, Pt and SBN. The in-plane orientation of ± 56^{o} can be described as SBN (001)/Pt (320)//MgO (320). In this orientation the lattice mismatch is about 14%. Also, there is still a possibility of in-plane rotation in ± 45^{o} with the in-plane alignment SBN (001)/Pt (220)//MgO (220), the lattice mismatch of such alignment is about 10 %.

Figure 8 shows the hysteresis loop of SBN thin film devices with different Gd-doping concentration, all the hysteresis measurements were under room temperature and pressure. The voltage was applied to the top and bottom laterally, the applied voltages were then converted to the lateral electric field by dividing the film thickness. The polarization was calculated by the measured polarization dividing by the junction area which is defined as the area crossed between top and bottom electrodes. **Table 2** summaries the remnant polarization P_r as a function of different Gd-doping concentration. The results show that P_r of the Gd-doped SBN thin films are similar to the P_r of the pure SBN film, except the 1% Gd doped film. Indeed, the 1 % Gd-doped film has a P_r value about 9 times larger than the undoped sample and 4 times larger than those of the other doped samples. Furthermore, we notice that the saturation polarization could not be showed clearly in Figure 8, and the shape of the hysteresis loop looks similar to a lossy capacitor, probably due to the leakage current. When the applied voltage was further increased, the ferroelectric junction was broken down and no ferroelectric signal was resulted. In order to withstand a large switching field and to prevent the breakdown of the film, the thickness of SBN thin film was doubled. **Figure 9** shows the hysteresis measurement of 500 nm Gd4%-SBN50 thin film. When the applied electric field was as large as 500 kVcm^{-2}, all the dipoles began to align with the field and reached the saturation polarization gradually. The measured P-E loop was right shifted and polarized asymmetrically because of the asymmetric top and bottom electrodes i.e the difference of work function of Pt bottom electrode and Au top electrode resulted in different polarization and coercive field [19] **Figure 10(a)** shows the frequency dependent relative dielectric constant measured at room temperature to estimate the capacitive frequency response of the ferroelectric junctions. The result shows that the doped SBN thin films generally possess higher relative dielectric constants compared with the undoped one, indicating that introducing rare-earth element increases the relative permittivity of the ferroelectric parallel plate capacitor. However, larger ε_r will usually accompany with larger dielectric loss as shown in **Figure 10(b)**. The relative permittivity was decreased slowly as the frequency increased, but as it

approached to about 100 MHz, the relative permittivity suddenly increased rapidly. As the doping concentrations increased, the turning point seemed to be shifted to lower frequency. The dispersion spectrum is important parameter for considering the device performance under various driving frequencies.

4. Conclusion

SBN thin films doped with different Gd doping concentrations were fabricated by pulsed laser deposition and characterized by XRD. XRD analysis showed that the SBN films had a c-axis oriented and epitaxial relationship with the (100) MgO substrate and Pt (001)/MgO (001) system. A right shift of SBN (002) peak position with an increasing of doping concentration was observed, indicating a contraction in the lattice length along the c-axis direction due to the replacement of Sr ions by the dopant ions. The ferroelectricity of the SBN thin film with different Gd-doped concentration was demonstrated using the Au/SBN/Pt multilayer system. Our results demonstrated that the SBN can be epitaxially grown on Pt-coated MgO substrates for further device applications.

Acknowledgements

This work was supported by the Natural Science Foundation of China (Grant No. 51502129), and The Hong Kong Polytechnic University (ZVGH and GUA5G)

Conflict of Interest

The authors declare no conflict of interest.

Received: ((will be filled in by the editorial staff))
Revised: ((will be filled in by the editorial staff))
Published online: ((will be filled in by the editorial staff))

Reference

1. Lenzo, P. V.; Spencer, E. G.; Ballman, A. A., Electro- Optic Coefficients of Ferroelectric Strontium Barium Niobate. *Applied Physics Letters* **1967,** *11* (1), 23-24.
2. Santos, I. A.; Garcia, D.; Eiras, J. A., Pyroelectric properties of rare earth doped strontium barium niobate ceramics from 20K to 450K. *Ferroelectrics* **2001,** *257* (1), 105-110.
3. Glass, A. M., Investigation of the Electrical Properties of Sr1−xBaxNb2O6 with Special Reference to Pyroelectric Detection. *Journal of Applied Physics* **1969,** *40* (12), 4699-4713.
4. Said, M.; Velayutham, T. S.; Gan, W. C.; Abd Majid, W. H., The structural and electrical properties of SrxBa(1−x)Nb2O6 (SBN) ceramic with varied composition. *Ceramics International* **2015,** *41* (5, Part B), 7119-7124.
5. Velayutham, T. S.; Salim, N. I. F.; Gan, W. C.; Abd. Majid, W. H., Effect of cerium addition on the microstructure, electrical and relaxor behavior of Sr 0.5 Ba 0.5 Nb 2 O 6 ceramics. *Journal of Alloys and Compounds* **2016,** *666*, 334-340.
6. Mak, C. L.; Lai, B.; Wong, K. H., Fabrication and Characterization of Sol-Gel Derived Potassium Sodium Strontium Barium Niobate. *Journal of Sol-Gel Science and Technology* **2000,** *18* (3), 225-233.
7. Yingbang, Y.; Leung, M. C.; Hung, W. K.; Shengguo, L.; Zhengkui, X., Effects of Rare-Earth Dopants on the Ferroelectric and Pyroelectric Properties of Strontium Barium Niobate Ceramics. *International Journal of Applied Ceramic Technology* **2009,** *6* (6), 671-678.
8. Vigne, S.; Hossain, N.; Fesharaki, F.; Kabir, S. M.; Margot, J.; Wu, K.; Chaker, M., Optical properties of epitaxial Ca_xBa_{1-x}Nb₂O₆ thin film based rib-waveguide structure on (001) MgO for electro-optic applications. *Opt Express* **2016,** *24* (25), 28573-28582.
9. Zhang, Y.; Tao, K.; Ma, Y.; Yang, S.; Wang, B.; Mak, C. L.; Wong, K. H., Growth and Optical Properties of (KNa)0.1(Sr0.61Ba0.39)0.9Nb2O6Thin Films by Pulsed Laser Deposition. *Japanese Journal of Applied Physics* **2007,** *46* (3A), 1063-1066.
10. Cuniot-Ponsard, M.; Desvignes, J. M.; Bellemain, A., Epitaxial growth of Sr x Ba1−x Nb2 O6 (SBN) thin films on Pt coated MgO substrates: the determining control of platinum crystallographic orientation. *Journal of Materials Science* **2006,** *41* (16), 5302-5309.
11. McIntyre, P. C.; Maggiore, C. J.; Nastasi, M., Orientation selection in thin platinum films on (001) MgO. *Journal of Applied Physics* **1995,** *77* (12), 6201-6204.

12. Yum, T.-Y.; Mak, C.-L.; Wong, K.-H., Fabrication and characterization of epitaxial Sr0.6Ba0.4Nb2O6/La0.7Sr0.3CoO3 heterostructures. *Applied Surface Science* **2006,** *252* (13), 4829-4833.
13. Willmott, P. R.; Herger, R.; Patterson, B. D.; Windiks, R., Experimental and theoretical study of the strong dependence of the microstructural properties ofSrxBa1−xNb2O6thin films as a function of their composition. *Physical Review B* **2005,** *71* (14).
14. Nonlinear optical properties of textured strontium barium niobate thin films prepared by metalorganic chemical vapor deposition. *Applied Physics Letters* **1995,** *66* (14), 1726-1728.
15. Yum, T.-Y.; Mak, C.; Wong, K.-H., *Fabrication and characterization of epitaxial Sr0.6Ba0.4Nb2O6/La0.7Sr0.3CoO3 heterostructures*. 2006; Vol. 252, p 4829–4833.
16. Li, X. T.; Du, P. Y.; Ye, H.; Mak, C. L.; Wong, K. H., Electro-optic properties of epitaxial Sr0.6Ba0.4Nb2O6 films grown on MgO substrates using LixNi2-xO buffer layer. *Applied Physics A* **2008,** *92* (2), 397-400.
17. Thöny, S. S.; Youden, K. E.; Jr., J. S. H.; Hesselink, L., Growth of epitaxial strontium barium niobate thin films by pulsed laser deposition. *Applied Physics Letters* **1994,** *65* (16), 2018-2020.
18. Lee, M.; Feigelson, R. S., Growth of epitaxial strontium barium niobate thin films by solid source metal-organic chemical vapor deposition. *Journal of Crystal Growth* **1997,** *180* (2), 220-228.
19. Toda, M. a. M., Asymmetric Hysteresis Loops, Leakage Current and Capacitance Voltage Behaviors in Ferroelectric PZT Films Deposited on a Pt/Al2O3/SiO2/Si Substrate by MOCVD method with a vapor-deposited Gold Top Electrode. *International Journal of Applied Physics and Mathematics* **2011,** *1* (2), 144-148.

((Insert Figure here. Note: Please do not combine figure and caption in a textbox or frame.))

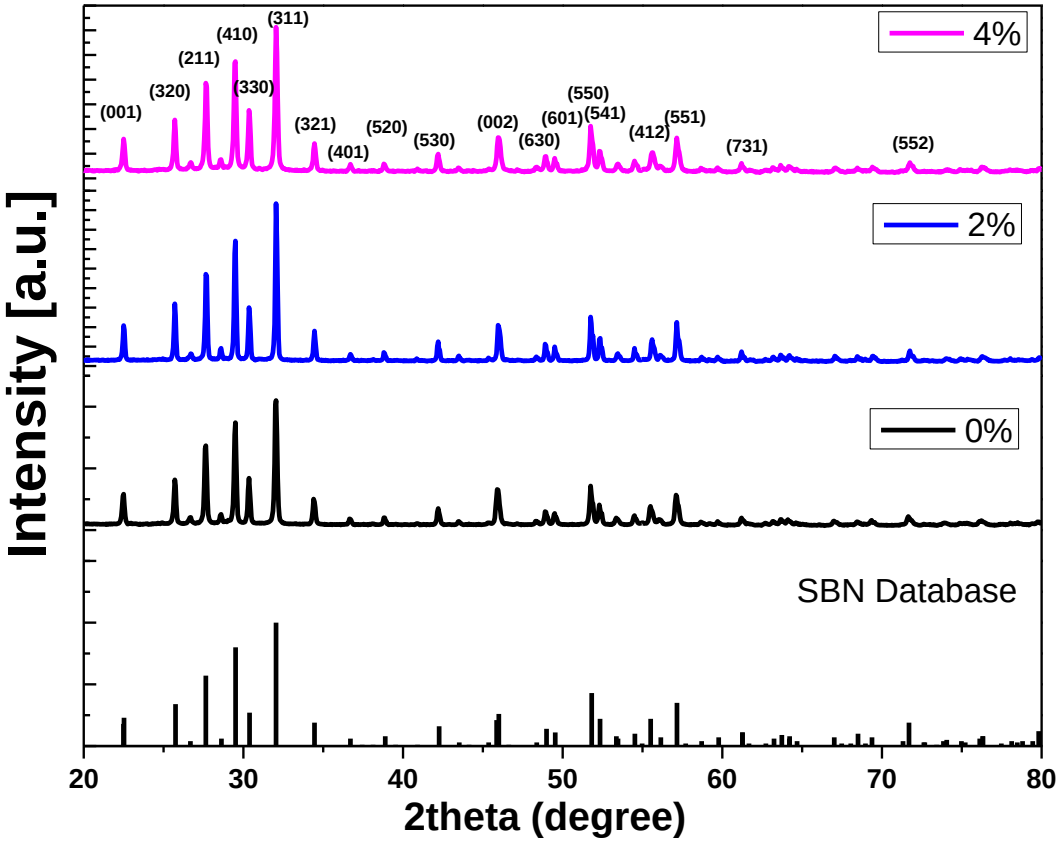

Figure 1. XRD spectra of pure SBN50 ceramic and SBN50 ceramic doped with 2% and 4% Gadolinium concentrations sintered at 1300 °C for 8 hours

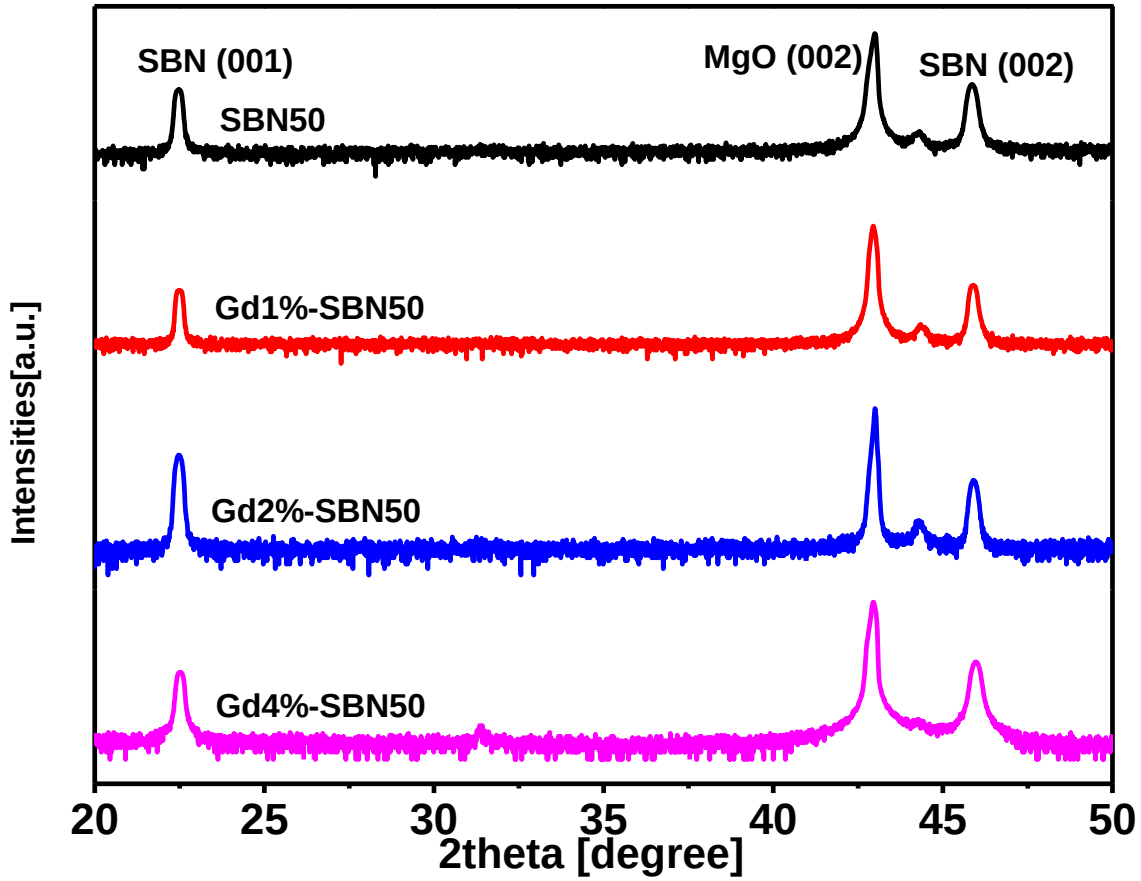

Figure 2 XRD spectra of pure SBN50 thin film and SBN50 ceramic doped with1 %, 2 % and 4 % Gd ions on MgO (001) substrate.

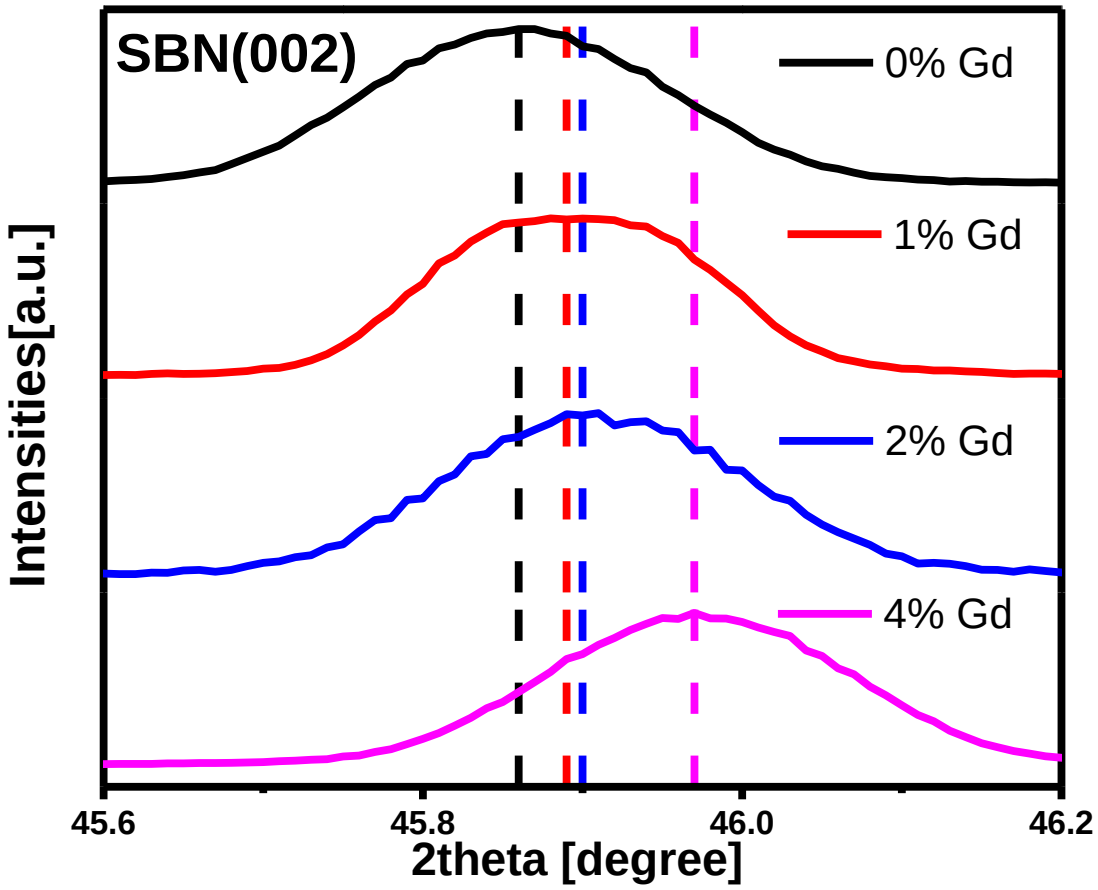

Figure 3.The shifting in SBN (002) diffraction angle with increasing Gd-concentration.

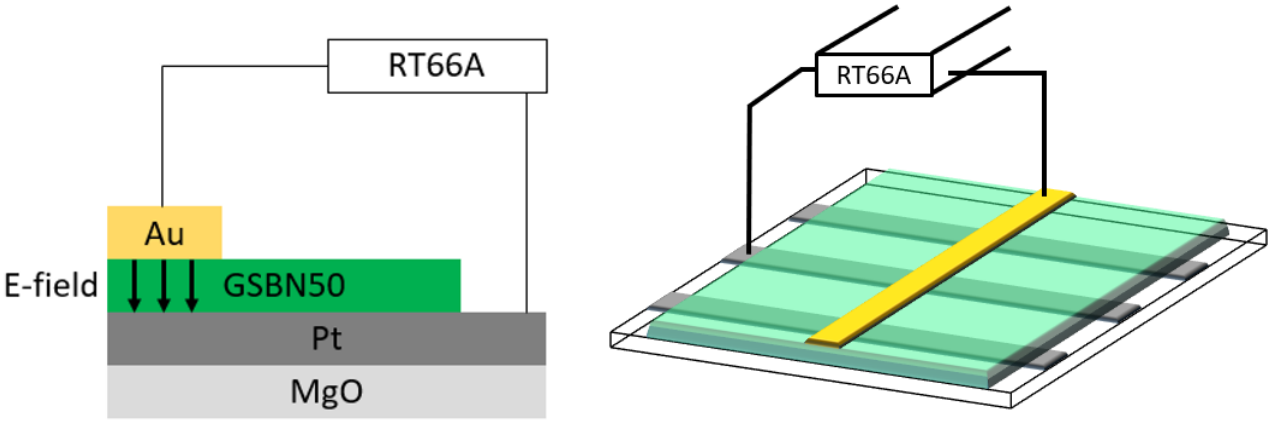

Figure 4. Schematic diagram of Au(50 nm)/ GSBN50(500 nm) /Pt(50 nm)/MgO device (left) and the 3D structure of crossed bottom and top electrode structure. (right)

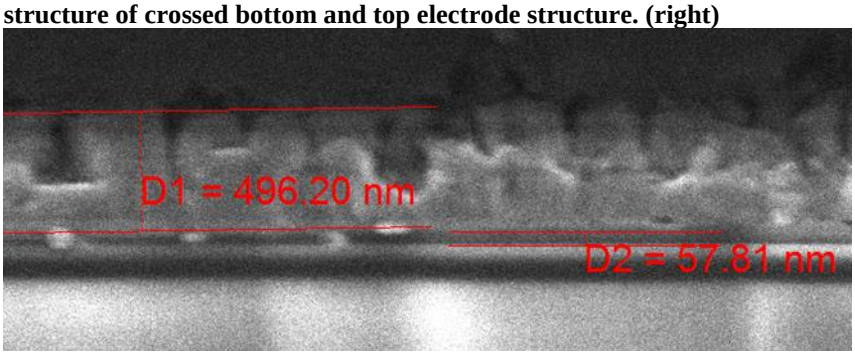

Figure 5. Cross-section FESEM image of SBN/Pt/MgO structure

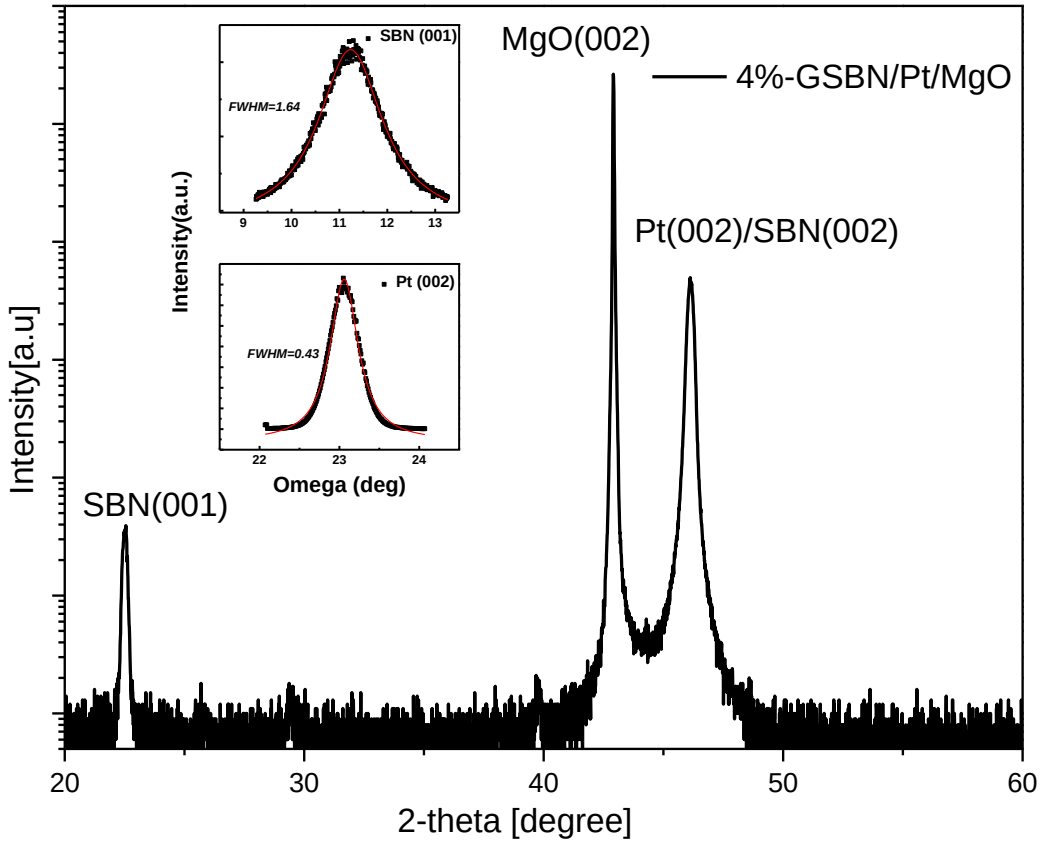

Figure 6 XRD *θ-2θ* scan of 4%-GSBN50(500 nm)/Pt(50 nm)/MgO multilayer structure. Inset: ω-scan of SBN (001) and Pt (002)/ SBN (002) diffraction peaks.

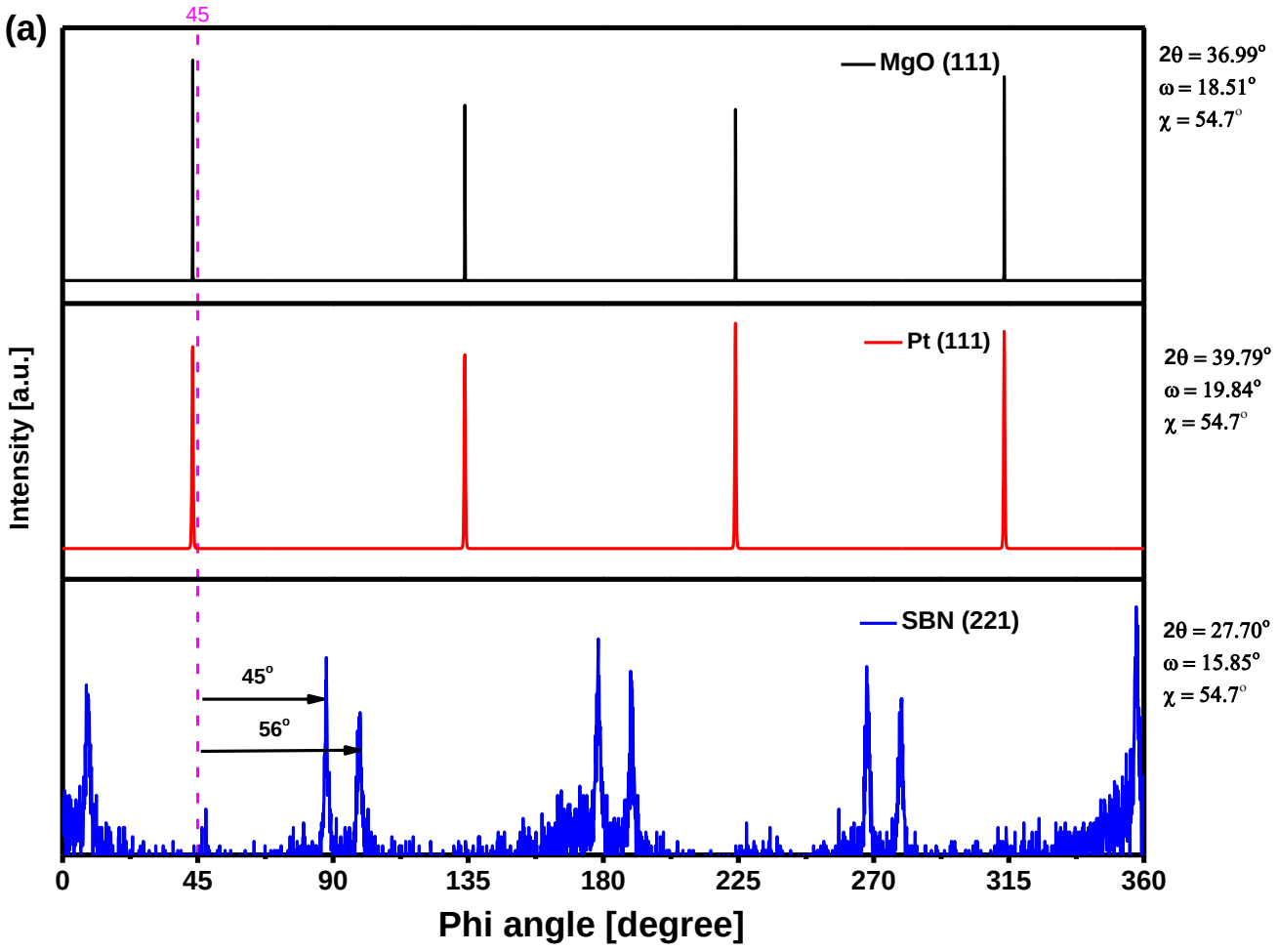

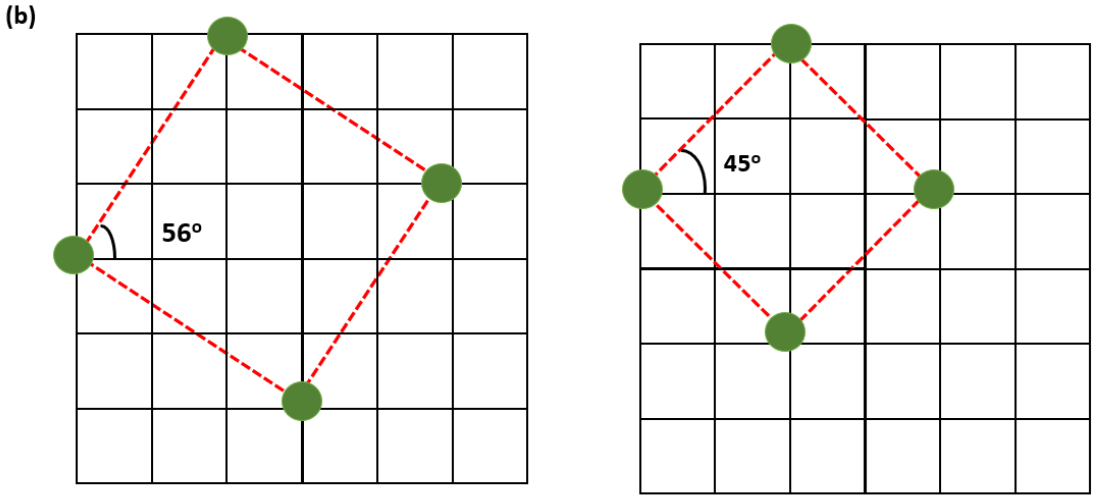

Figure 7(a.) XRD phi scan showing epitaxial in-plane relationship of MgO(substrate)/Pt(film)/SBN(film). The substrate tilting at Chi-angle= 54.7°. (b.) Schamatic diagram of in-plane orientation of SBN on Pt thim film.

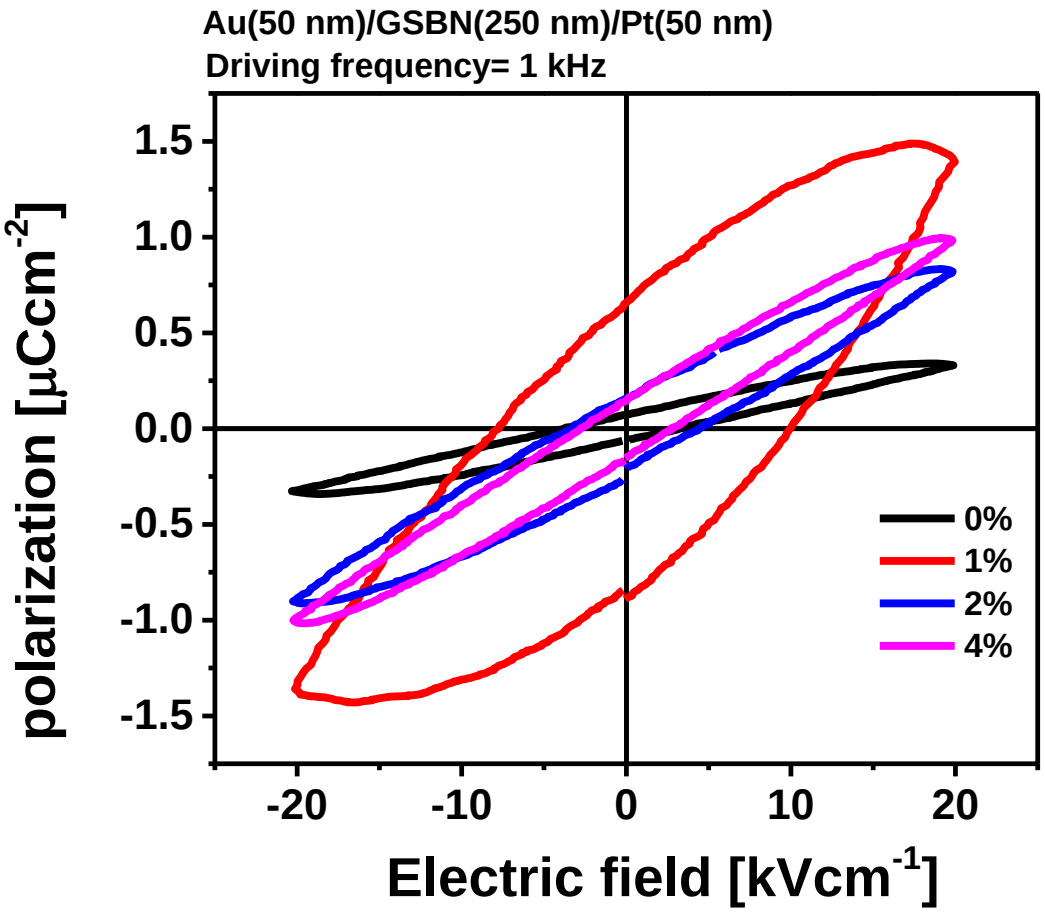

Figure 8 P-E hysteresis loops of undoped SBN and doped with Gd film measured at 1 kHz with applied an electric field, E =20 kV/cm.

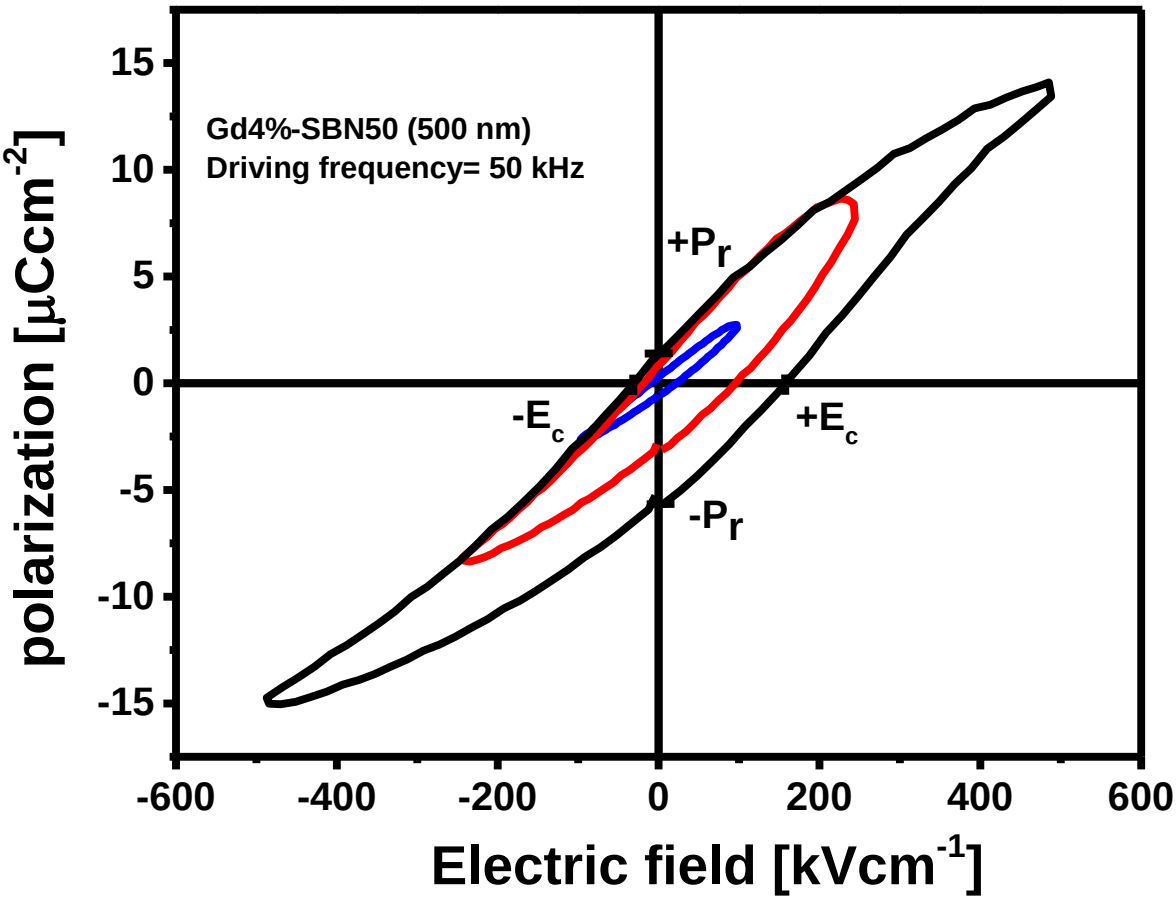

Figure 9 The P-E hysteresis loop of 4 % Gd-doped SBN thin film with the varied electric field.

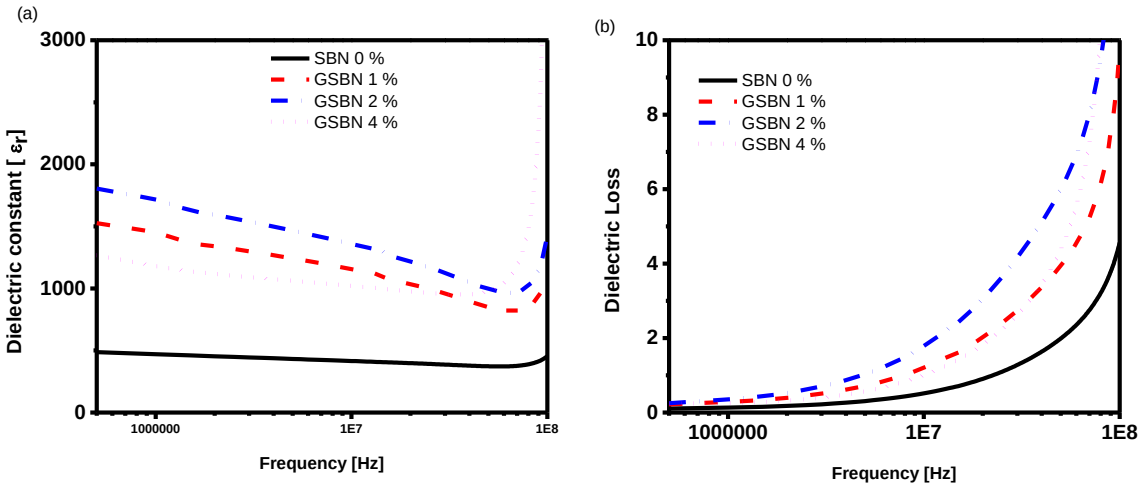

Figure 10 Frequency dependence of the relative dielectric constant ε_r and dielectric loss of the different Gd doped SBN thin film grown on Pt/ MgO substrate.

Table 1 Calculated value C-lattice constant against the doping concentration

Sample	C-lattice constant [nm]
SBN50	0.3952
Gd-1% SBN50	0.3950
Gd-2% SBN50	0.3949
Gd-4% SBN50	0.3943

Table 2 The coercive field (E_c) and remnant polarization (P_r) as a function of the Gd-doping concentration

Sample	Coercive field [$kVcm^{-1}$]	Remnant polarization [μCcm^{-2}]
SBN50	3.25	0.07
Gd-1 % SBN50	9.94	0.66
Gd-2 % SBN50	4.46	0.16
Gd-4 % SBN50	2.72	0.14

((**For Essays, Feature Articles, Progress Reports, and Reviews,** please insert up to three author biographies and photographs here, max. 100 words each))

Author Photograph(s) ((40 mm broad, 50 mm high, gray scale))

The table of contents entry should be 50–60 words long, and the first phrase should be bold. The entry should be written in the present tense and impersonal style. The text should be different from the abstract text.

Keyword

$Sr_{0.5}Ba_{0.5}Nb_2O_{6,}$ Pulsed laser deposition, Ferroelectricity

Title ((no stars))

ToC figure ((Please choose one size: 55 mm broad × 50 mm high **or** 110 mm broad × 20 mm high. Please do not use any other dimensions))